ACS Sustainable Chemistry & Engineering

Letter

pubs.acs.org/journal/ascecg

Reduced Graphene Oxide (rGO)/$BiVO_4$ Composites with Maximized Interfacial Coupling for Visible Lght Photocatalysis

Tuo Wang, Changjiang Li, Junyi Ji, Yijia Wei, Peng Zhang, Shengping Wang, Xiaobin Fan, and Jinlong Gong*

Key Laboratory for Green Chemical Technology of Ministry of Education, School of Chemical Engineering and Technology, Collaborative Innovation Center of Chemical Science and Engineering, Tianjin University, Tianjin 300072, China

Supporting Information

ABSTRACT: This paper describes the construction of reduced graphene oxide (rGO)/$BiVO_4$ composites with maximized interfacial coupling and their application as visible light photocatalysts. Thin rGO sheets (<5 nm) could completely cover $BiVO_4$ polyhedrons with highly active (040) facets exposed through an evaporation-induced self-assembly process. In addition to the increased surface adsorption effect of rGO, a considerable enhancement of the photoactivity of $BiVO_4$ has been demonstrated through the degradation of methylene blue upon the covering of rGO. The improved photocatalytic activity is attributed to the formation of well-defined rGO/$BiVO_4$ interfaces, which greatly enhances the charge separation efficiency.

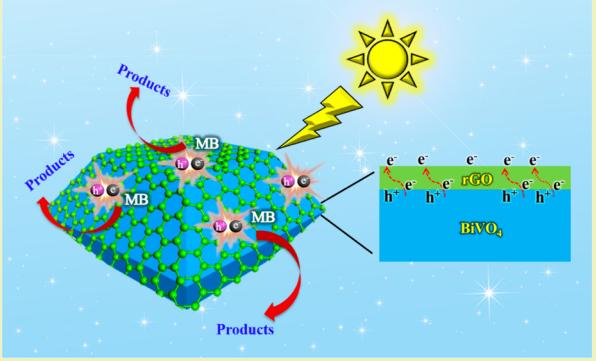

KEYWORDS: *Reduced graphene oxide (rGO), $BiVO_4$, Interface, Charge separation, Visible light photocatalysis, Photocatalytic degradation*

INTRODUCTION

Photocatalysis has received considerable attention for its potential to solve the energy crisis and environmental pollution by using solar energy.[1] Up to now, the practical uses of photocatalysts were mainly hindered by low charge separation efficiency and poor visible light response.[2] Visible light photocatalysts with superior activity have been widely exploited to achieve the ultimate goal of using solar energy directly.[3,4]

Monoclinic bismuth vanadate (m-$BiVO_4$) with excellent visible light response and good chemical stability has been elegantly applied in water splitting and pollutant degradation.[5,6] The exposed crystal facets have great effects on the photocatalytic activities of $BiVO_4$. For example, $BiVO_4$ with (040) facets exposed has presented superior photocatalytic performances.[7−9] Also, different facets in well-defined $BiVO_4$ polyhedrons exhibit synergistic effects to form functional facets, which demonstrates that facet modification could be an effective strategy to design photocatalysts, especially for $BiVO_4$ polyhedrons.[10,11] However, surface properties of $BiVO_4$ such as fast charge recombination at surfaces and weak surface adsorption ability have greatly limited further improvement of its photocatalytic activity.[5,12]

Reduced graphene oxide (rGO) with excellent electrical conductivity and high carrier mobility has been proved to be an excellent media for electron transfer.[13] A large number of rGO-based photocatalysts have been successfully constructed for enhanced photocatalytic performances.[14,15] Among them, rGO/$BiVO_4$ composites have attracted much attention with significant progress achieved.[16−18] For example, Amal and colleagues showed that GO can be reduced by light-induced electrons of $BiVO_4$.[19] It is expected that well-defined rGO/$BiVO_4$ interfaces that can ensure the timely transfer of electrons are significantly important to achieve efficient charge separation. Also, a full coverage of rGO sheets on $BiVO_4$ surfaces is preferred to thoroughly overcome the surface charge recombination.[20,21] Previous work mainly employed rGO as the support of $BiVO_4$, and few reports have focused on tuning the interface between rGO and $BiVO_4$. Moreover, rGO/$BiVO_4$ composites with rGO sheets completely covering $BiVO_4$ polyhedrons with highly active (040) facets exposed for maximized phase coupling have been rarely reported. This paper describes the construction of rGO/$BiVO_4$ composites, which is featured by thin rGO sheets (<5 nm) completely covering $BiVO_4$ polyhedrons with (040) facets exposed, achieving maximized interfacial coupling between rGO and $BiVO_4$ for increased charge separation efficiency (as illustrated in Figure 1).

EXPERIMENTAL SECTION

Sample Synthesis. $BiVO_4$ polyhedrons with (040) facets exposed were first synthesized through a surfactant-assisted hydrothermal method. Subsequently, the GO/$BiVO_4$ composites were constructed

Received: July 18, 2014
Revised: August 15, 2014
Published: August 21, 2014

   dx.doi.org/10.1021/sc5004665 | ACS Sustainable Chem. Eng. 2014, 2, 2253−2258

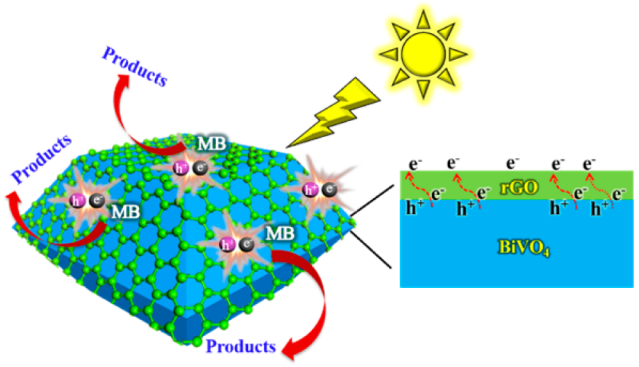

Figure 1. Schematic illustration of rGO/$BiVO_4$ with a thin rGO sheet (<5 nm) conformally covering a $BiVO_4$ polyhedron, forming a well-defined interface for enhanced charge separation efficiency.

through an evaporation-induced self-assembly process between $BiVO_4$ polyhedrons and GO sheets. The GO/$BiVO_4$ composites were then transformed to rGO/$BiVO_4$ composites through a mild and green visible light-stimulated photocatalytic reduction process without using any toxic reagents (e.g., hydrazine). The detailed synthesis processes can be found in the Supporting Information.

Physicochemical Characterizations. The as-synthesized samples were investigated by powder X-ray diffraction recorded with a Bruker D8 Focus operating at 40 kV and 40 mA equipped with nickel-filtered Cu Kα radiation (λ = 1.54056 Å) and operated in a 2θ range of 10–80° at a scanning rate of 0.02° per step. Field emission-scanning electron microscopy (FE-SEM) images were obtained using a Hitachi S-4800 SEM at 5 kV. Transmission electron microscope (TEM) images were obtained using a JEM-2100F TEM at 200 kV. Raman spectra of the samples were recorded with a Raman spectrometer (DXR Microscope), and a green semiconductor laser (532 nm) was used as the excitation source. UV–vis diffuse reflectance spectra (DRS) of the as-prepared samples were obtained using a Shimadzu UV-2550 spectrophotometer equipped with an integrating sphere using $BaSO_4$ as the reflectance standard. X-ray photoelectron spectroscopy (XPS) analysis of the sample was carried out on a Physical Electronics PHI 1600 ESCA system operated at a pass energy of 187.85 eV with an Al Kα X-ray source (E = 1486.6 eV), and all binding energies of the composing elements were referenced to the C 1s peak at 284.6 eV. Photoluminescence (PL) spectra were obtained with a fluorescence spectrophotometer (Hitachi, F-4500) with an excitation wavelength of 325 nm at room temperature.

Photocatalytic Activity Measurements. Photocatalytic activities of the samples were evaluated by the degradation of methylene blue (MB) solution under visible light ($\lambda \geq$ 420 nm) in a homemade reactor with a cooling water circulator assembled to keep the reactor at a constant temperature. In detail, 50 mg of catalysts was dispersed into 100 mL MB solution (10 mg/L), and the suspension was sonicated for 5 min followed by magnetically stirring for 30 min in the dark condition to make sure the establishment of an adsorption–desorption equilibrium before irradiation. A 300 W xenon lamp with a 420 nm cutoff filter to remove any irradiation below 420 nm was used as the visible light source to trigger the photocatalytic reaction. At certain time intervals, the reaction solution was sampled and centrifuged to remove catalysts to test the intensity changes of the absorption peak at 664 nm to determine the concentration of MB at different times by the same UV–vis spectrophotometer (UV-2550, Shimadzu, Japan).

Photoelectrochemical Tests. Electrochemical impedance spectra (EIS) and Mott–Schottky (MS) plots were obtained using a three-electrode configuration with the as-prepared electrodes as the working electrode, saturated Ag/AgCl as the reference electrode, and platinum foil as the counter electrode. A 0.1 M Na_2SO_4 solution was used as the electrolyte. Impedance measurements were performed in the dark in a Na_2SO_4 solution (0.1 M) at open circuit voltage over a frequency range from 100 kHz to 0.1 Hz with an AC voltage at 50 mV. Mott–Schottky plots were obtained at a fixed frequency of 2 kHz in the dark.

RESULTS AND DISCUSSION

The as-synthesized $BiVO_4$ polyhedrons show a well-defined truncated bipyramid shape with highly active (040) facets exposed, and all $BiVO_4$ surfaces are smooth without impurities adhered (Figure 2a). In rGO/$BiVO_4$ composites, rGO sheets

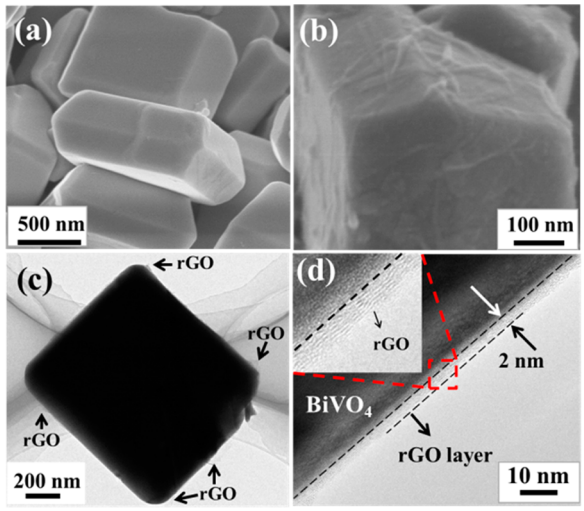

Figure 2. SEM images of as-synthesized samples: (a) $BiVO_4$ with smooth surface, (b) rGO/$BiVO_4$ with rGO layer uniformly attached on $BiVO_4$ forming a wrinkled surface, and (c,d) TEM images of rGO/$BiVO_4$ exhibiting a tight contact between $BiVO_4$ and the rGO layer (about 2 nm).

are uniformly attached on $BiVO_4$ surfaces through an evaporation-induced self-assembly process to form rGO/$BiVO_4$ composites with wrinkled surfaces (Figure 2b). We obtain TEM images of rGO/$BiVO_4$ composites to further characterize the structure of rGO/$BiVO_4$ and the interface between rGO and $BiVO_4$. In a single rGO/$BiVO_4$ polyhedron (Figure 2c), the rGO layer can only be observed in certain positions (see arrows) because of the tight contact between $BiVO_4$ and rGO, which is consistent with the SEM results. A typical magnified TEM image (Figure 2d) reveals that the rGO layer with a thickness about 2 nm is tightly attached on $BiVO_4$ surfaces to form well-defined phase interfaces. Statistical results show that the thicknesses of rGO layers are below 5 nm, and only in a few places, the rGO thickness can increase to 10 nm due to the aggregation of rGO layers. In essence, rGO and $BiVO_4$ can form well-defined rGO/$BiVO_4$ interfaces, and no free-hanging rGO sheets can be observed (Figure S3, Supporting Information). The reduction of GO and the evaporation process force the rGO sheets to assemble on the surface of $BiVO_4$ particles conformally. When we increase the starting GO amount to 2.5 wt %, the SEM images show that excess rGO sheets are agglomerated without attaching on $BiVO_4$ (Figure S4, Supporting Information), indicating that the current GO loading (1.5 wt %) is appropriate to form rGO/$BiVO_4$ composites with rGO sheets wrapping on $BiVO_4$ polyhedrons. To test the stability of the rGO/$BiVO_4$ structures, we treated the samples by ultrasound for 30 min. The SEM image (Figure S5, Supporting Information) shows that the rGO/$BiVO_4$ structures remain intact after ultrasonication, which demonstrates the excellent stability of the rGO/$BiVO_4$ structures.

XRD pattern (Figure 3a) shows that the as-synthesized $BiVO_4$ has a monoclinic scheelite phase (JCPDS No.14-0688),

dx.doi.org/10.1021/sc5004665 | ACS Sustainable Chem. Eng. 2014, 2, 2253–2258

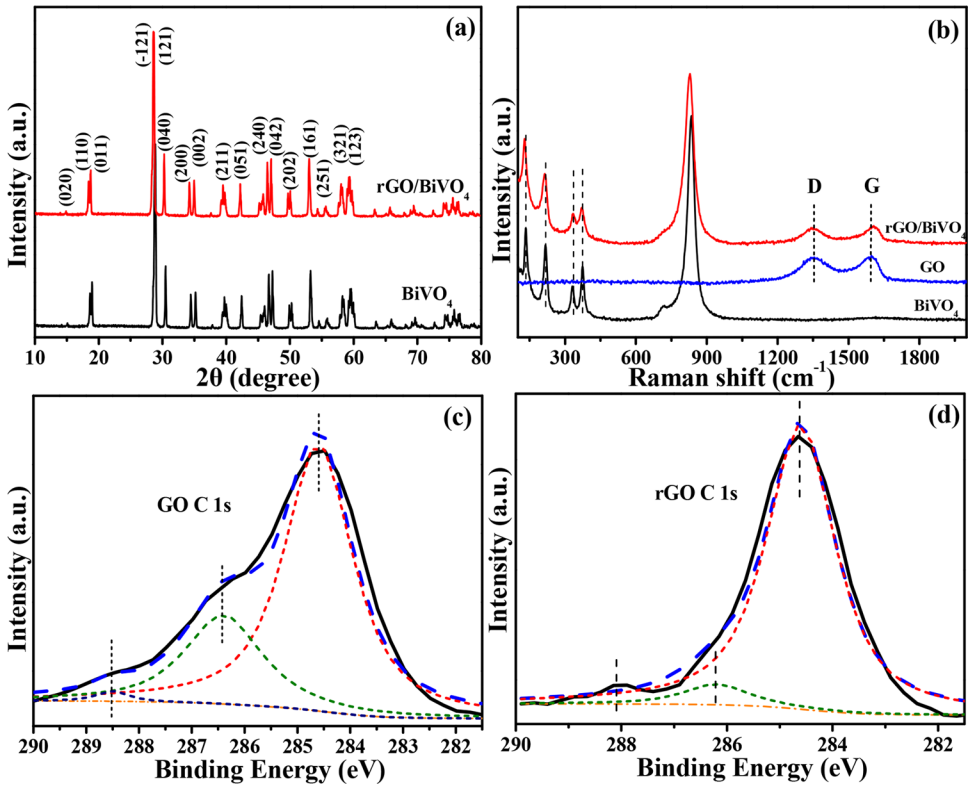

Figure 3. (a) XRD patterns of as-synthesized samples indicating the high crystallinity of monoclinic $BiVO_4$ and the successful reduction of GO to rGO. (b) Raman spectra of the as-synthesized samples demonstrating the monoclinic phase of and confirming the reduction of GO through the shift of D and G bands. (c) C 1s XPS spectrum of GO/$BiVO_4$. (d) C 1s XPS spectrum of rGO/$BiVO_4$ exhibiting a significant decrease of the C−O band, indicating the reduction of GO to rGO.

which is the most active phase among the three phases of $BiVO_4$.[22,23] The sharp XRD peaks indicate the high crystallinity of $BiVO_4$. The XRD pattern of the rGO/$BiVO_4$ composite is similar to that of $BiVO_4$, and no characteristic peak of GO at around 12° can be found, indicating that GO has been reduced to rGO through the photocatalytic reduction process. Comparatively, when the amount of GO increases to 2.5 wt %, XRD result shows that GO cannot be completely reduced to rGO upon the same reduction process (Figure S6, Supporting Information). These results suggest that the unique GO/$BiVO_4$ structure with well-defined interfaces is not only favorable to charge transfer but also beneficial to the photocatalytic reduction of GO. Consistent with XRD results, Raman spectra (Figure 3b) demonstrate that $BiVO_4$ has a monoclinic phase based on the characteristic stretching vibrations and bending vibrations of VO_4^{3-} tetrahedron.[11] The Raman spectrum of GO/$BiVO_4$ shows two characteristic bands at 1355 and 1597 cm^{-1}, corresponding to the D band and G band of GO, respectively. Comparatively, in rGO/$BiVO_4$ composites, the D band and G band are slightly blue- and red-shifted to 1346 and 1606 cm^{-1}, respectively, which may be caused by the changed surface strain due to the contact between rGO and $BiVO_4$.[24] XPS spectra were obtained to further prove the reduction of GO to rGO by detecting the chemical state of C species.[19] The characteristic peaks of C 1s in GO/$BiVO_4$ can be ascribed to the sp^2 bonded carbon (C−C) species (~284.6 eV), C−OH species (~286.4 eV), and C═O−OH species (~288.6 eV) (Figure 3c). Upon photocatalytic reduction, the peak intensity of C−O bonds in C 1s XPS spectrum significantly decreases (Figure 3d), indicating that GO has been well reduced to rGO by light-induced electrons[19] favored by the intimate contacts to achieve effective electron transfer as described above.

UV−vis spectra are used to characterize the optical properties of the samples (Figure 4). It is apparent that pure

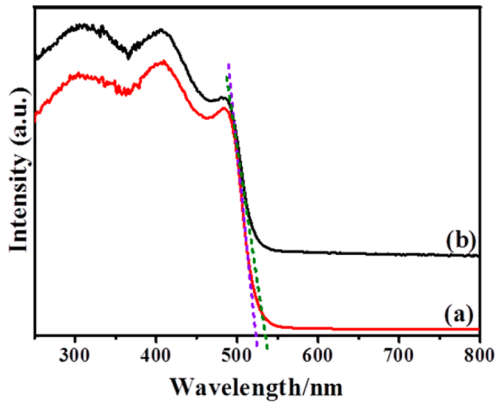

Figure 4. UV−vis spectra of samples (a) $BiVO_4$ and (b) rGO/$BiVO_4$ composite, exhibiting similar absorption edges and close absorption intensities below 500 nm, ensuring the adequate photoexcitation of $BiVO_4$ covered by a thin rGO sheet.

$BiVO_4$ exhibits an absorption edge at around 520 nm, showing good visible light response. For the rGO/$BiVO_4$ composite, the absorption edge slightly red-shifted to around 530 nm, and the light absorption ability in the range of 550−800 nm is also increased due to the absorption of rGO. The similar absorption edge of the two samples indicates that a thin rGO sheet does not compete with $BiVO_4$ significantly for light below 520 nm,

dx.doi.org/10.1021/sc5004665 | ACS Sustainable Chem. Eng. 2014, 2, 2253−2258

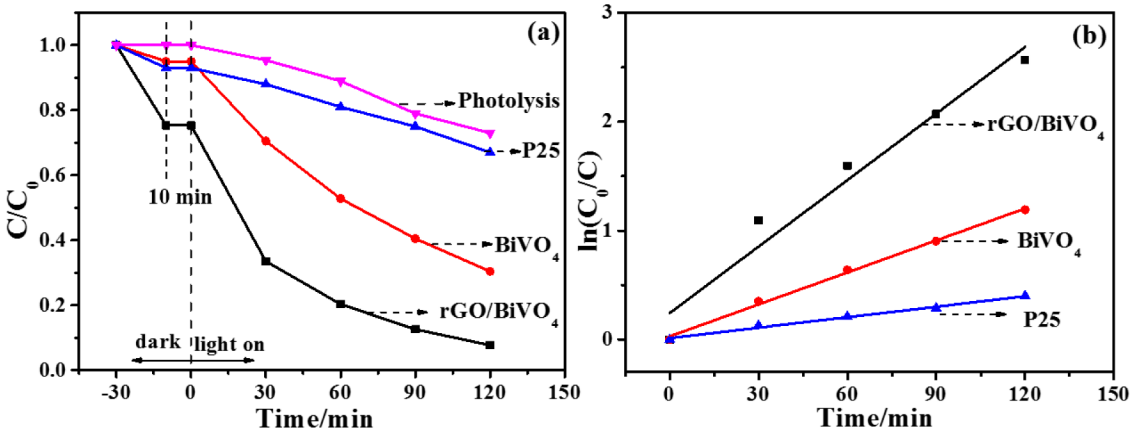

Figure 5. (a) Photocatalytic degradation of MB under the irradiation of visible light ($\lambda \geq 420$ nm) over the samples, where rGO/$BiVO_4$ degrades 94% of MB within 120 min, much higher than pure $BiVO_4$ (70% of MB in 120 min). (b) The $\ln(C_0/C)$ as a function of irradiation time (t) for MB degradation, where rGO/$BiVO_4$ exhibits a k value (0.021 min^{-1}) 2.14 times as high as that of $BiVO_4$ (0.0098 min^{-1}).

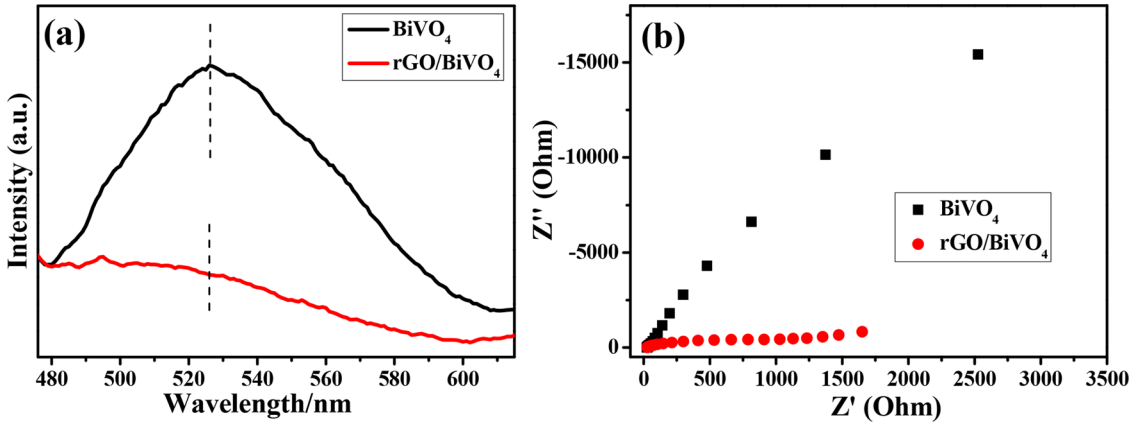

Figure 6. (a) Photoluminescence spectra suggesting the suppression of undesirable charge recombination upon the formation of rGO/$BiVO_4$ composites. (b) Electrochemical impedance spectra (in Nyquist plots) implying the reduced charge transfer resistance and recombination rate of $BiVO_4$ upon the formation of rGO/$BiVO_4$ composites.

and the absorption intensities of the two samples below 500 nm are fairly close, ensuring an adequate photoexcitation in $BiVO_4$ covered by a rGO sheet.

Photocatalytic activities of the as-prepared photocatalysts were evaluated by photocatalytic degradation of MB under the irradiation of visible light ($\lambda \geq 420$ nm) (Figure 5a). Photolysis and Degussa P25 were used as comparisons. All suspensions were first stirred in the dark for 30 min before irradiation to reach adsorption−desorption equilibrium as confirmed by the steady-state concentrations in the last 10 min of dark stirring. We can clearly observe that photolysis and P25 cannot degrade MB prominently within 120 min, which can exclude the effects of self-degradation of MB and the existence of UV light. When using pure $BiVO_4$ as the photocatalyst, 70% of MB is degraded in 120 min, while the rGO/$BiVO_4$ composite can degrade 94% of MB within 120 min, exhibiting greatly enhanced photocatalytic activity as compared to pure $BiVO_4$. The kinetics of the photocatalytic reactions can be regarded as a pseudo-first-order reaction mode because the concentration of the MB solution is relatively low (10 mg/L)[6], and k values are estimated from the linear regression of $\ln(C_0/C)$ vs irradiation time (t) (Figure 5b). The rGO/$BiVO_4$ composite shows the highest k value of 0.021 min^{-1}, which is about 2.14 times as high as that of $BiVO_4$ (0.0098 min^{-1}). In addition to the increased surface adsorption of MB enabled by rGO, the 2.14 times enhancement after irradiation suggests a considerable strengthening effect of the photoactivity of $BiVO_4$ upon the covering of rGO.

We propose that the enhanced photocatalytic activity can be ascribed to the increased charge separation efficiency. To prove this, we obtained PL spectra and EIS and MS plots of the samples. The PL emission intensity of rGO/$BiVO_4$ composites is much weaker than that of $BiVO_4$ (Figure 6a), indicating that the energy-wasting and undesirable charge recombination process is greatly suppressed upon the formation of rGO/$BiVO_4$ composites. Also, from EIS (in the form of Nyquist plots, Figure 6b), it is observed that the semicircle of rGO/$BiVO_4$ is much smaller than that of pure $BiVO_4$, demonstrating that the charge transfer resistance of $BiVO_4$ is significantly decreased upon the formation of rGO/$BiVO_4$ composites, implying a greatly reduced recombination rate.[25] Furthermore, the MS plot (Figure S7, Supporting Information) of rGO/$BiVO_4$ shows a much smaller slope than that of $BiVO_4$, which can further confirm the increased charge separation efficiency.[25] From above analysis, we can conclude that the as-synthesized rGO/$BiVO_4$ composites show substantially increased charge separation efficiency favored by the maximized interfacial coupling. The high electrical conductivity of rGO makes it an excellent acceptor for photogenerated electrons.[24] Upon the formation of well-defined rGO/$BiVO_4$ interfaces, rGO could promote a fast separation of photocarriers by removing

electrons from $BiVO_4$. To prove the effective transfer of separated electrons to reactants at the other side of a rGO sheet, visible light-induced Au deposition on a rGO/$BiVO_4$ surface was conducted. The results show that Au nanoparticles are evenly dispersed on rGO surfaces (Figure S8, Supporting Information), indicating that electrons can transfer from $BiVO_4$ to rGO surfaces where they are captured by reactants. Furthermore, the enhanced surface adsorption ability of rGO/$BiVO_4$ composites and the exposed highly active $BiVO_4$ (040) facets can also account for the excellent photocatalytic activity of the rGO/$BiVO_4$ composites.[26]

CONCLUSIONS

In conclusion, we have successfully constructed rGO/$BiVO_4$ composites with maximized interfacial coupling by fully covering rGO sheets on $BiVO_4$ polyhedrons through an evaporation-induced self-assembly process. In the rGO/$BiVO_4$ composites, $BiVO_4$ polyhedrons show a well-defined truncated bipyramid shape with (040) facets exposed, and the rGO layers conformally cover $BiVO_4$ polyhedron surfaces to form well-defined rGO/$BiVO_4$ interfaces. The as-prepared rGO/$BiVO_4$ composites present significantly increased charge separation efficiency and enhanced surface adsorption ability, leading to greatly improved photocatalytic activity for degradation of MB under visible light. This work may provide new opportunities for the construction of efficient rGO-based photocatalysts. Moreover, considering the potential of $BiVO_4$ for photocatalytic oxidation of water for O_2,[9] the rGO/$BiVO_4$ catalyst is expected to have applicability in water splitting and CO_2 reduction.

ASSOCIATED CONTENT

Supporting Information

Detailed sample synthesis processes, photographs of sample solution and electrodes, SEM images of as-synthesized GO, rGO/$BiVO_4$ prepared from excess GO loading, rGO/$BiVO_4$ after ultrasound treatment, Au-rGO/$BiVO_4$ composite, TEM images of rGO/$BiVO_4$, XRD pattern of rGO/$BiVO_4$, Mott–Schottky plots. This material is available free of charge via the Internet at http://pubs.acs.org.

AUTHOR INFORMATION

Corresponding Author

*E-mail: jlgong@tju.edu.cn. Fax: (+86) 22-87401818.

Notes

The authors declare no competing financial interest.

ACKNOWLEDGMENTS

This work was supported by the National Science Foundation of China (21222604, 51302185), Program for New Century Excellent Talents in University (NCET-10-0611), Scientific Research Foundation for the Returned Overseas Chinese Scholars (MoE), and Program of Introducing Talents of Discipline to Universities (B06006).

REFERENCES

(1) Fujishima, A.; Honda, K. Electrochemical photolysis of water at a semiconductor electrode. *Nature* **1972**, *238*, 37–38.

(2) Tong, H.; Ouyang, S.; Bi, Y.; Umezawa, N.; Oshikiri, M.; Ye, J. Nano-photocatalytic materials: Possibilities and challenges. *Adv. Mater.* **2012**, *24*, 229–251.

(3) Zhang, P.; Zhang, J.; Gong, J. Tantalum-based semiconductors for solar water splitting. *Chem. Soc. Rev.* **2014**, *43*, 4395–4422.

(4) Park, Y.; McDonald, K. J.; Choi, K. S. Progress in bismuth vanadate photoanodes for use in solar water oxidation. *Chem. Soc. Rev.* **2013**, *42*, 2321–2337.

(5) Kim, T. W.; Choi, K. S. Nanoporous $BiVO_4$ photoanodes with dual-layer oxygen evolution catalysts for solar water splitting. *Science* **2014**, *343*, 990–994.

(6) Li, C.; Wang, S.; Wang, T.; Wei, Y.; Zhang, P.; Gong, J. Monoclinic porous $BiVO_4$ networks decorated by discrete g-C_3N_4 nano-islands with tunable coverage for highly efficient photocatalysis. *Small* **2014**, *10*, 2783–2790.

(7) Wang, D.; Jiang, H.; Zong, X.; Xu, Q.; Ma, Y.; Li, G.; Li, C. Crystal facet dependence of water oxidation on $BiVO_4$ sheets under visible light irradiation. *Chem.—Eur. J.* **2011**, *17*, 1275–1282.

(8) Yang, J.; Wang, D.; Zhou, X.; Li, C. A theoretical study on the mechanism of photocatalytic oxygen evolution on $BiVO_4$ in aqueous solution. *Chem.—Eur. J.* **2013**, *19*, 1320–1326.

(9) Xi, G.; Ye, J. Synthesis of bismuth vanadate nanoplates with exposed {001} facets and enhanced visible-light photocatalytic properties. *Chem. Commun.* **2010**, *46*, 1893–1895.

(10) Li, R.; Zhang, F.; Wang, D.; Yang, J.; Li, M.; Zhu, J.; Zhou, X.; Han, H.; Li, C. Spatial separation of photogenerated electrons and holes among {010} and {110} crystal facets of $BiVO_4$. *Nat. Commun.* **2013**, *4*, 1432.

(11) Li, C.; Zhang, P.; Lv, R.; Lu, J.; Wang, T.; Wang, S.; Wang, H.; Gong, J. Selective deposition of Ag_3PO_4 on monoclinic $BiVO_4$ (040) for highly efficient photocatalysis. *Small* **2013**, *9*, 3951–3956.

(12) Saison, T.; Chemin, N.; Chaneac, C.; Durupthy, O.; Ruaux, V.; Mariey, L.; Mauge, F.; Beaunier, P.; Jolivet, J. P. Bi_2O_3, $BiVO_4$, and Bi_2WO_6: Impact of surface properties on photocatalytic activity under visible light. *J. Phys. Chem. C* **2011**, *115*, 5657–5666.

(13) Li, N.; Liu, G.; Zhen, C.; Li, F.; Zhang, L. L.; Cheng, H. M. Battery performance and photocatalytic activity of mesoporous anatase TiO_2 nanospheres/graphene composites by template-free self-assembly. *Adv. Funct. Mater.* **2011**, *21*, 1717–1722.

(14) Tan, L. L.; Chai, S. P.; Mohamed, A. R. Synthesis and applications of graphene-based TiO_2 photocatalysts. *ChemSusChem* **2012**, *5*, 1868–1882.

(15) Huang, X.; Qi, X. Y.; Boey, F.; Zhang, H. Graphene-based composites. *Chem. Soc. Rev.* **2012**, *41*, 666–686.

(16) Yan, Y.; Sun, S.; Song, Y.; Yan, X.; Guan, W.; Liu, X.; Shi, W. Microwave-assisted in situ synthesis of reduced graphene oxide-$BiVO_4$ composite photocatalysts and their enhanced photocatalytic performance for the degradation of ciprofloxacin. *J. Hazard. Mater.* **2013**, *250–251*, 106–114.

(17) Fu, Y.; Sun, X.; Wang, X. $BiVO_4$–Graphene catalyst and its high photocatalytic performance under visible light irradiation. *Mater. Chem. Phys.* **2011**, *131*, 325–330.

(18) Sun, Y.; Qu, B.; Liu, Q.; Gao, S.; Yan, Z.; Yan, W.; Pan, B.; Wei, S.; Xie, Y. Highly efficient visible-light-driven photocatalytic activities in synthetic ordered monoclinic $BiVO_4$ quantum tubes-graphene nanocomposites. *Nanoscale* **2012**, *4*, 3761–3767.

(19) Ng, Y. H.; Iwase, A.; Kudo, A.; Amal, R. Reducing graphene oxide on a visible-light $BiVO_4$ photocatalyst for an enhanced photoelectrochemical water splitting. *J. Phys. Chem. Lett.* **2010**, *1*, 2607–2612.

(20) Yang, J.; Heo, M.; Lee, H. J.; Park, S. M.; Kim, J. Y.; Shin, H. S. Reduced graphene oxide (rGO)-wrapped fullerene (C60) wires. *ACS Nano* **2011**, *5*, 8365–8371.

(21) Wang, C.; Meng, D.; Sun, J.; Memon, J.; Huang, Y.; Geng, J. Graphene wrapped TiO_2 based catalysts with enhanced photocatalytic activity. *Adv. Mater. Interfaces* **2014**, DOI: 10.1002/admi.201300150.

(22) Kudo, A.; Omori, K.; Kato, H. A novel aqueous process for preparation of crystal form-controlled and highly crystalline $BiVO_4$ powder from layered vanadates at room temperature and its photocatalytic and photophysical properties. *J. Am. Chem. Soc.* **1999**, *121*, 11459–11467.

(23) Tokunaga, S.; Kato, H.; Kudo, A. Selective preparation of monoclinic and tetragonal $BiVO_4$ with scheelite structure and their photocatalytic properties. *Chem. Mater.* **2001**, *13*, 4624–4628.

(24) Sang, Y.; Zhao, Z.; Tian, J.; Hao, P.; Jiang, H.; Liu, H.; Claverie, J. P. Enhanced photocatalytic property of reduced graphene oxide/TiO_2 nanobelt surface heterostructures constructed by an in situ photochemical reduction method. *Small* **2014**, DOI: 10.1002/smll.201303489.
(25) Su, F.; Wang, T.; Lv, R.; Zhang, J.; Zhang, P.; Lu, J.; Gong, J. Dendritic Au/TiO_2 nanorod arrays for visible-light driven photoelectrochemical water splitting. *Nanoscale* **2013**, *5*, 9001−9009.
(26) Liu, J. H.; Wang, Z. C.; Liu, L. W.; Chen, W. Reduced graphene oxide as capturer of dyes and electrons during photocatalysis: Surface wrapping and capture promoted efficiency. *Phys. Chem. Chem. Phys.* **2011**, *13*, 13216−13221.